Centrifuge Modeling of the Dynamic Response of an Embankment: LEAP-ASIA 2025 Tests at Kyoto University

S. Ohashi
Graduate School of Engineering, Kyoto University, Kyoto, Japan, ohashi.shunsuke.47p@st.kyoto-u.ac.jp

N. Takamatsu
Graduate School of Engineering, Kyoto University, Kyoto, Japan, takamatsu.nao.76v@st.kyoto-u.ac.jp

K. Ueda
Disaster Prevention Research Institute, Kyoto University, Kyoto, Japan, ueda.kyohei.2v@kyoto-u.ac.jp

ABSTRACT: This study reports the results of centrifuge model tests conducted using the centrifuge facility of the Disaster Prevention Research Institute (DPRI), Kyoto University, as part of LEAP-ASIA-2025. A series of shaking tests was performed on a double-sided embankment model with a prototype height of 5 m constructed on liquefiable sandy ground. To evaluate the effects of friction at the front and back walls, two test conditions (with and without sheets) were examined. The influence of the embankment on the liquefiable ground was investigated based on measurements of acceleration, pore water pressure, laser displacement, and CPT results. The results showed notable differences in acceleration and CPT responses between the two conditions, whereas no significant differences were observed in the excess pore water pressure ratio or the vertical displacement at the crest of the embankment. Future work will include a comparison of acceleration data in terms of frequency characteristics and numerical simulation results, as well as additional experiments and improvements to visualization techniques to enhance measurement accuracy.

1 INTRODUCTION

LEAP (Liquefaction Experiments and Analysis Projects) is an international project established to ensure the generality of results and to contribute to improving the accuracy of ground failure predictions through coordinated experiments using centrifuge facilities and coordinated analyses using various model configurations. For LEAP-ASIA-2025, a model was specified in which a 5-m-high double-sided embankment at prototype scale is placed on a 10-m-deep foundation soil. The main objective is to evaluate the performance of existing numerical analysis methods for liquefaction under complex stress conditions, such as initial shear stress and various overburden pressures. As part of this project, centrifuge model tests were conducted using the centrifuge facility at the Disaster Prevention Research Institute (DPRI), Kyoto University.

In centrifuge model tests, it is ideally assumed—particularly from the perspective of two-dimensional numerical analysis—that the ground behavior within the soil container does not vary in the out-of-plane (depth) direction, i.e., that plane-strain conditions apply. However, friction along the container walls may cause differences between the behavior of soil near the walls and that inside the soil mass. Methods using sheets or grease have been proposed to mitigate this effect (Takahashi et al., 2018). Therefore, the objective of this study is to evaluate the influence of embankments on liquefiable soil and to investigate the effect of wall friction by comparing shaking results between cases with and without sheets.

2 CENTRIFUGE MODEL

Figure 1 shows the dimensions and instrumentation of the model. At the prototype scale, the embankment has a height of 5 m, a base length of 20.35 m, a crest length of 3 m, and a slope angle of 30 degrees, while the foundation has a depth of 10 m and a width of 38.5 m.

2.1 Generalized scaling law

The centrifuge facility at Kyoto University has an upper limit of 50G for dynamic experiments, which restricts the achievable model scale. Simply applying a centrifugal acceleration of 50G would result in a 1/50 model scale, requiring a ground width of 0.77 m. However, the maximum allowable container width under dynamic loading at the Kyoto University

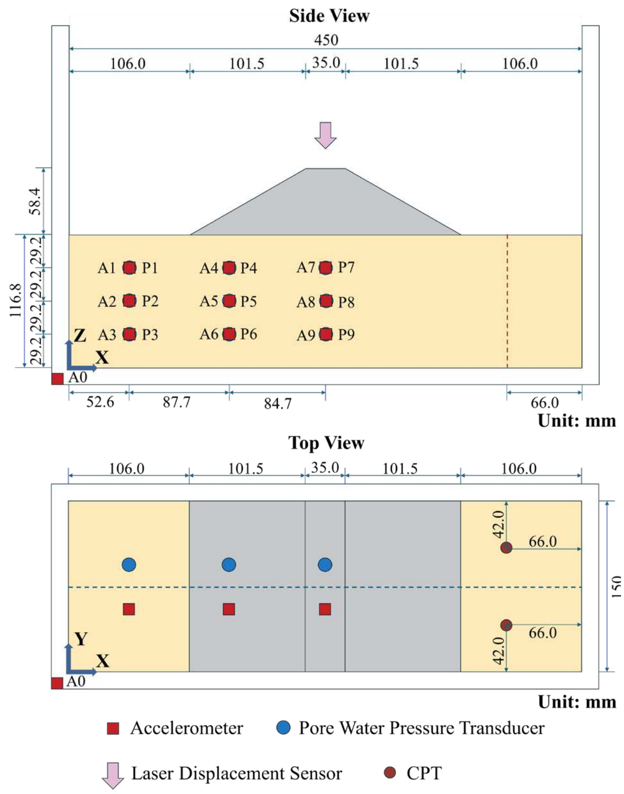

Figure 1. Dimensions and instrumentation of the model.

centrifuge is 0.61 m, making such an experiment infeasible.

Therefore, the generalized scaling law (Iai et al., 2005) was adopted in this study. In this approach, the prototype is first scaled down to a virtual 1G model by applying the scaling law for 1G shaking table tests (hereafter referred to as the scaling factor μ). In the second step, the virtual 1G model is further scaled down to a centrifuge model by applying the centrifuge scaling law (hereafter referred to as the scaling factor η). By multiplying these two scaling factors, a much larger overall model scale can be achieved than would be possible using conventional centrifuge scaling alone. The scaling factors adopted in this study are summarized in Table 1.

2.2 Description of the model

A rigid soil container with internal dimensions of 45 cm (width) × 30 cm (height) × 15 cm (depth) was used in the experiments. The front wall of the container was transparent, allowing observation of ground deformation. To record the input earthquake motion, a horizontal accelerometer (A0) was installed outside the container. In addition, nine horizontal accelerometers (A1–A9) and nine pore water pressure transducers (P1–P9) were installed within the foundation ground.

To investigate the effect of wall friction on seismic behavior, two experimental cases were conducted:

- Case A: with sheets
- Case B: without sheets

In Case A, Mobilon sheets coated with a mixture of silicone oil and grease were attached to the inner walls of the container in order to minimize friction between the container walls and the ground.

In this study, Ottawa F65 sand (ρ_{max} =1753 kg/m^3, ρ_{min} =1451 kg/m^3) was used as the foundation ground material, and Mizunami silica sand No. 4 was used for the embankment.

2.3 Model preparation

The foundation ground and the embankment were prepared separately. The preparation procedure is described below.

2.3.1 Foundation ground

The foundation ground was prepared using the air pluviation method. Prior to each experiment, Ottawa F65 sand was placed in a plastic bottle container, and

Table 1. Scaling factors.

	Scaling factors for 1G test	Scaling factors for centrifuge test	Generalized scaling factors	In these tests $\mu = 1.71$ $\eta = 50$
Length	μ	η	$\mu\eta$	85.6
Density	1	1	1	1
Time	$\mu^{0.75}$	η	$\mu^{0.75}\eta$	74.8
Frequency	$\mu^{-0.75}$	$1/\eta$	$\mu^{-0.75}/\eta$	0.013
Acceleration	1	$1/\eta$	$1/\eta$	0.02
Velocity	$\mu^{0.75}$	1	$\mu^{0.75}$	1.50
Displacement	$\mu^{1.5}$	η	$\mu^{1.5}\eta$	111.9
Stress	μ	1	μ	1.71
Strain	$\mu^{0.5}$	1	$\mu^{0.5}$	1.31
Stiffness	$\mu^{0.5}$	1	$\mu^{0.5}$	1.31
Permeability	$\mu^{0.75}$	η	$\mu^{0.75}\eta$	74.8
Pore pressure	μ	1	μ	1.71
Tip resistance	μ	1	μ	1.71

the sand was dropped into a mold through a perforated cap using the air pluviation method. The volume and mass of the deposited sand were then measured to calibrate the relationship between drop height and relative density, and an appropriate drop height was determined to achieve a target relative density of 60%.

In preparing the foundation ground, the same plastic bottle container was used, and sand was pluviated from the calibrated drop height so that each layer had a uniform thickness of 29.2 mm. At predetermined locations within each layer, three accelerometers and three pore water pressure transducers were installed. This procedure was repeated by adjusting the drop height and depositing sand until the foundation ground was completed.

Before preparing the foundation ground, in Case A, a mixture of silicone oil (KF-96-10CS, Shin-Etsu Chemical Co., Ltd.) and grease (KS-64, Shin-Etsu Chemical Co., Ltd.) in a 1:1 ratio was applied to the front and back walls of the soil container, and Mobilon sheets were attached. In contrast, no such treatment was applied in Case B.

2.3.2 Saturation Process

After constructing the foundation ground using the air pluviation method, the rigid container was placed in a vacuum chamber. In the initial stage, a vacuum pressure of approximately −0.09 MPa was applied and maintained until saturation process in order to promote the dissolution and removal of entrapped air bubbles.

Under this vacuum condition, a degassed mixed solution of water and methyl cellulose (SM-100, Shin-Etsu Chemical Co., Ltd.) was injected from the ground surface of the soil container over a period of approximately 6 hours to achieve full saturation. The mixing ratio of water and methyl cellulose was repeatedly adjusted until the target viscosity determined by the scaling law was achieved. Here, since the similitude ratio for the permeability coefficient is given as $\mu^{0.75}\eta = 74.8$, the target viscosity was set to be 74.8 times that of water.

The degree of saturation of the model was estimated using the Okamura method (Okamura and Inoue, 2012), which relates small fluctuations in the water surface induced by pressure changes to the degree of saturation. The instruments used for measuring the degree of saturation were pore water pressure transducers and a laser displacement sensor. Specifically, the soil container saturated with pore fluid was placed inside a vacuum chamber, and a target was floated on the water surface. The displacement of the water surface caused by applying negative pressure inside the vacuum chamber was measured using the laser displacement sensor. The degree of saturation was determined by calculating

Table 2. Overview of the two experimental cases.

	D_r	PGA	Sheets	S_r
Case A	60%	0.2G	With	99.1%
Case B	60%	0.2G	Without	97.6%

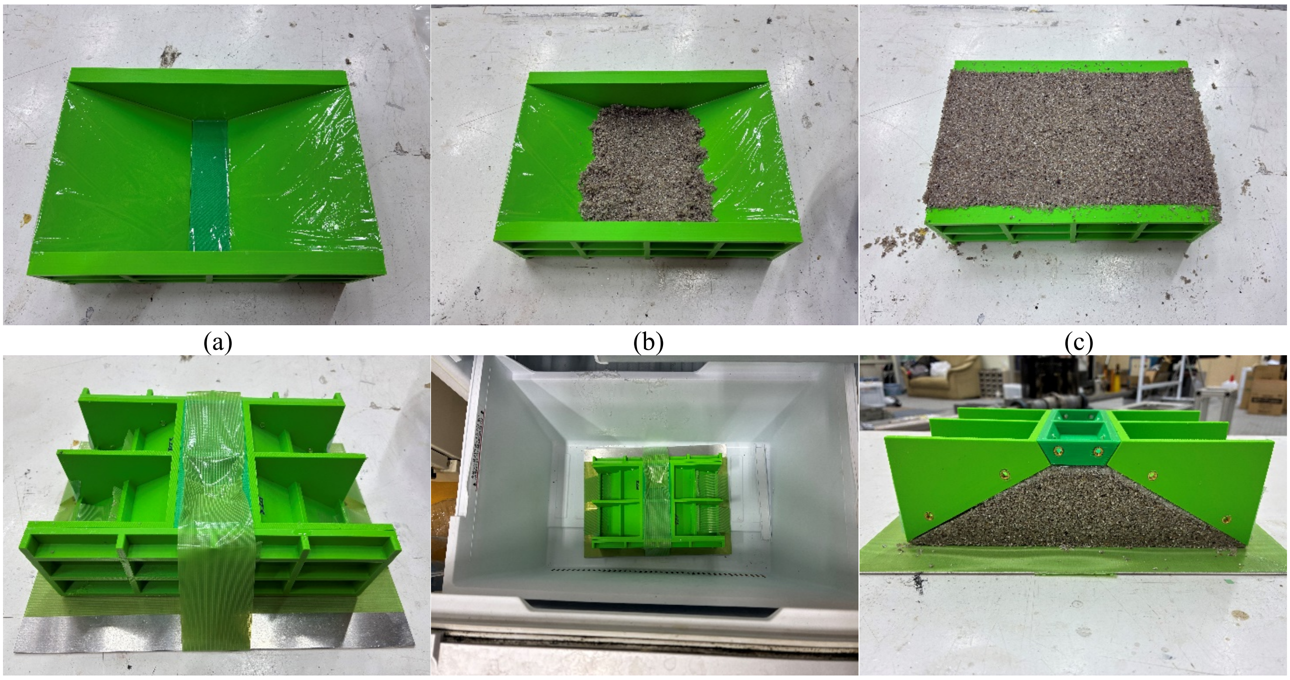

(d) (e) (f)

Figure 2. Preparation of the embankment: (a) plastic wrap was placed, (b) compacted in four layers, (c) entire prepared soil, (d) covered with a plate, (e) frozen overnight, and (f) completed embankment.

the volume of air remaining in the model ground from the relationship between the rate of pressure change and the corresponding change in the water surface level. An overview of the two experimental cases, including the measured degrees of saturation, is summarized in Table 2.

2.3.3 Embankment

The embankment was prepared following the procedure shown in Figure 2. A 3D-printed mold was used to prepare the embankment model, with a top length of 35 mm, a base length of 238 mm, a height of 58.4 mm, and a depth of 140 mm. The embankment model was inverted, and plastic wrap was placed on the upper surface of the embankment. A soil mixture consisting of No. 4 silica sand and a methyl cellulose solution was prepared and compacted in four layers so as to achieve a water content of 11.1% and a wet density of 1.7 g/cm³. By placing the entire prepared soil into the mold, the target water content and wet density were achieved. After compaction, the bottom of the embankment

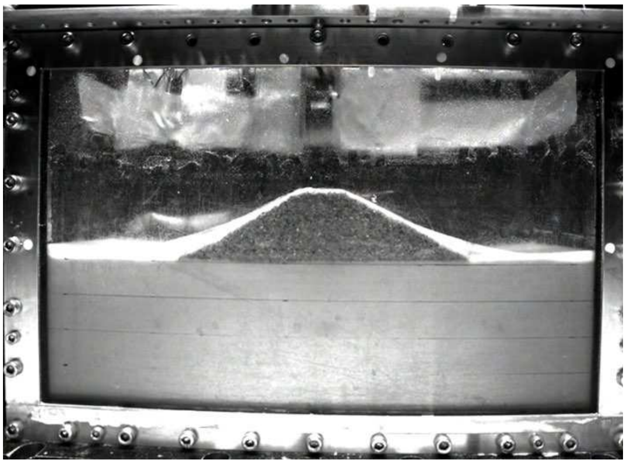

(a)

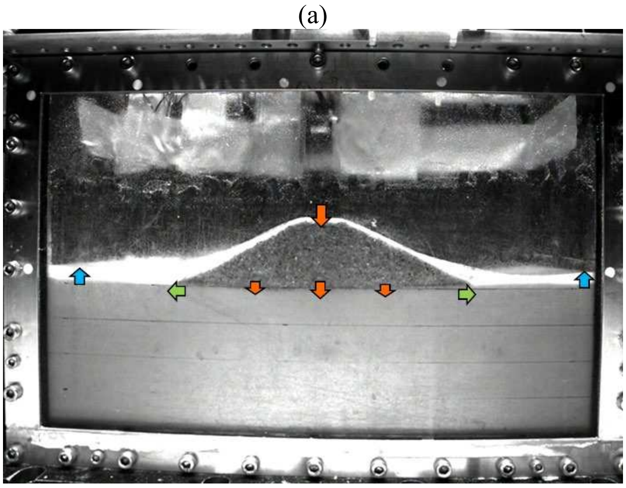

(b)

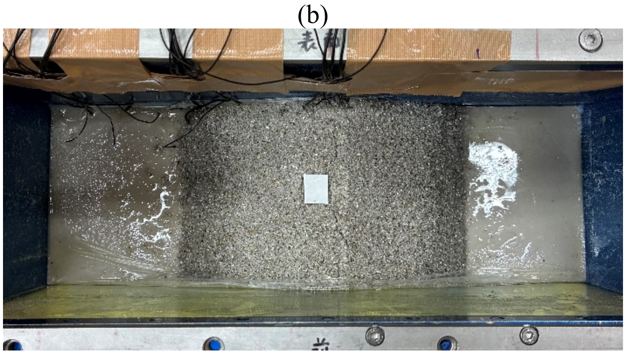

(c)

Figure 3. (a) Pre-shaking side view, (b) post-shaking side view, and (c) post-shaking top view (Case A).

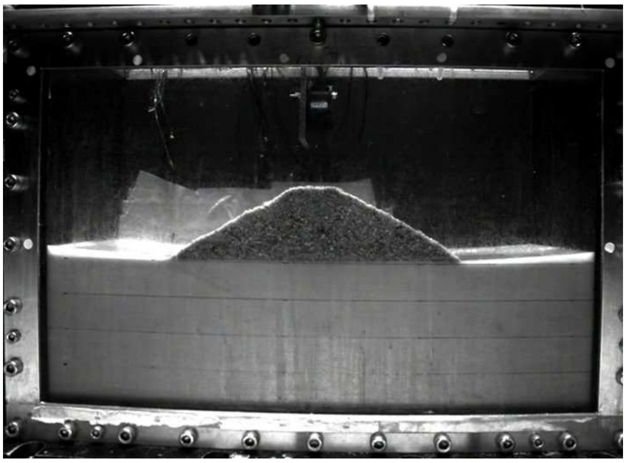

(a)

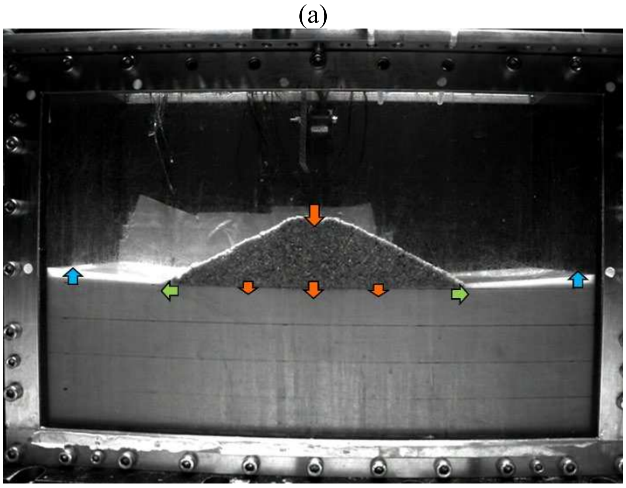

(b)

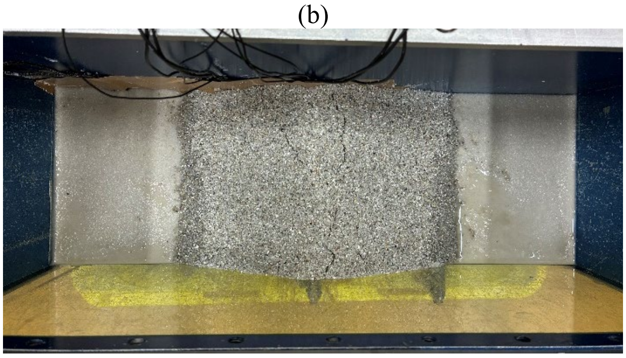

(c)

Figure 4. (a) Pre-shaking side view, (b) post-shaking side view, and (c) post-shaking top view (Case B).

model was covered with a plate, and the model was placed in a household freezer and frozen overnight.

After saturation, the embankment was placed at the center of the container, and the gap between the embankment and the container walls was filled with No. 4 silica sand. The model was then installed on the shaking table of the centrifuge apparatus.

2.4 Test procedure

First, the centrifugal acceleration was increased to 50G, and a CPT (cone penetration test) was conducted prior to shaking. The CPT is a test method used to continuously evaluate the engineering properties of the ground. After completion of the CPT, the centrifuge rotation was stopped, and the CPT device was replaced with a laser displacement sensor. Shaking was then performed under the same centrifugal acceleration of 50G. After the shaking was completed and drainage had finished, the centrifuge rotation was stopped again, the laser displacement sensor was replaced with the CPT device, and a second CPT was conducted.

3 TEST RESULTS

Figures 3 and 4 show the conditions of the model before and after shaking for Case A and Case B. Although careful interpretation is required because the scaling factors for length and displacement are not identical under the generalized scaling law, the embankment was observed to settle while spreading laterally. The settlement was greatest at the center of the embankment, and after shaking, the bottom surface of the embankment exhibited a curved shape.

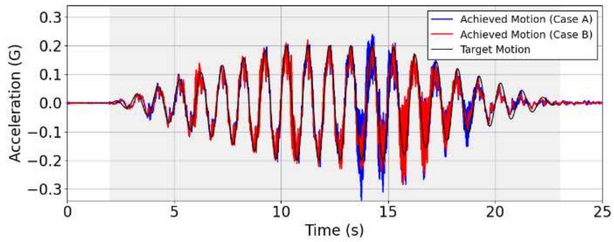

Figure 5. Comparison between the target input motion and the achieved input motion.

In addition, uplift of the free-field ground was observed after shaking. From a top view, cracks were identified at the crest of the embankment.

The results obtained from the accelerometers, pore water pressure transducers, laser displacement sensors, and CPT tests are presented below. In the time-history plots, the 21-second duration of shaking is highlighted in gray.

3.1 Achieved input motions

Figure 5 shows a comparison between the target input motion and the achieved input motion for each case. The target input motion was a sinusoidal wave in which the amplitude gradually increased from the start of shaking, remained constant for 5 seconds at a maximum amplitude of 0.2 G, and then gradually decreased. The frequency was 1 Hz, and the total duration was 21 seconds.

It can be observed that the amplitude becomes noticeably larger from approximately 10 seconds after the start of shaking.

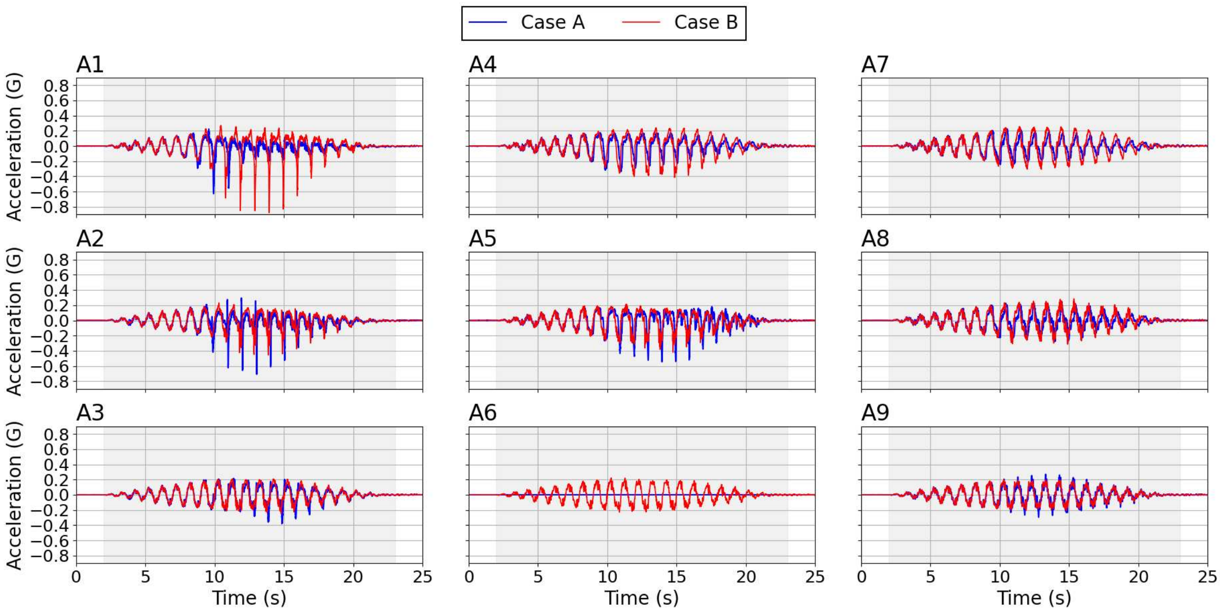

Figure 6. Ground motion acceleration.

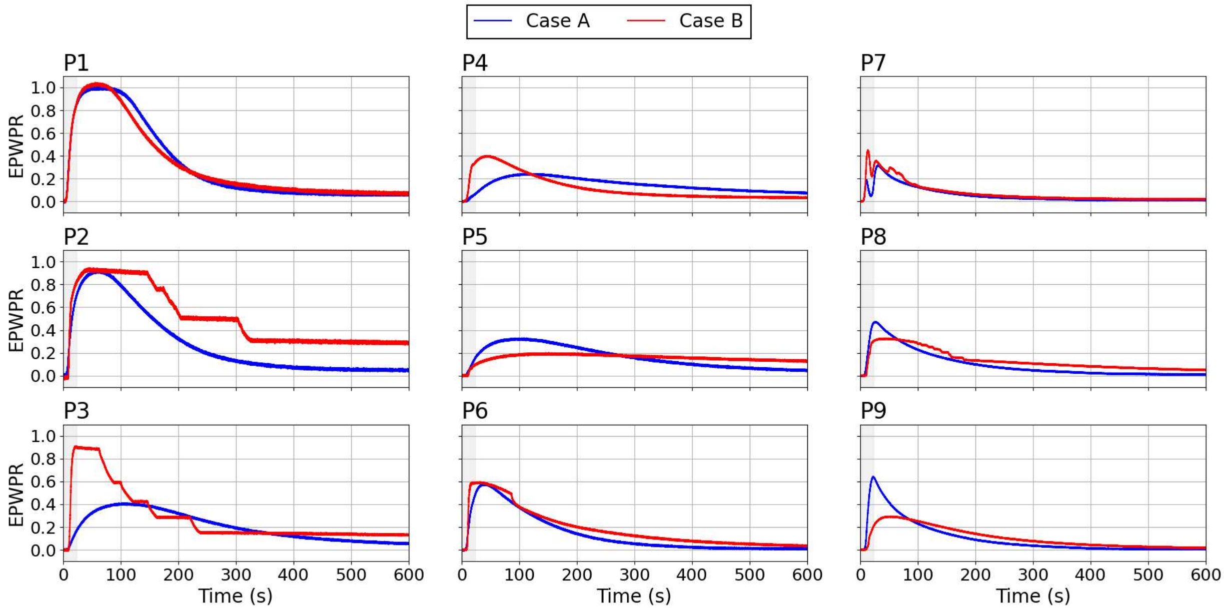

Figure 7. Excess pore water pressure ratio.

3.2 Ground motion accelerations

Figure 6 shows the acceleration records obtained from the nine accelerometers embedded in the soil. It should be noted that no valid data were obtained from A6 in Case A.

In the lower layer (A3, A6, and A9), Case B exhibited acceleration amplitudes comparable to the input motion, whereas Case A showed slightly larger amplitudes at A3 and A9. In contrast, at the locations beneath the embankment (A7 and A8), the amplitudes in Case A were nearly identical to those of the input motion, while Case B recorded noticeably larger accelerations.

Distinct spike-like acceleration responses were observed at A1, A2, A4 and A5. The spike at A1 and A4 was particularly prominent in Case B, whereas those at A2 and A5 were more pronounced in Case A. These spikes may indicate localized deformation or stiffness changes within the soil.

Focusing on the initial shear stress induced by the embankment, the acceleration amplitudes decrease in the order of A1, A4, and A7, and also in the order of A2, A5, and A8, indicating that the acceleration amplitude tends to decrease as the initial shear stress increases. At locations with smaller initial shear stress, liquefaction is more likely to occur, and consequently acceleration spikes, which are considered to be associated with cyclic mobility, are observed.

3.3 Excess pore water pressure ratio (EPWPR)

Figure 7 shows the time histories of the excess pore water pressure ratio calculated from the measurements obtained by the nine pore water pressure transducers installed in the ground. The excess pore water pressure ratio at each measurement point was calculated by dividing the excess pore water pressure at the corresponding depth by the initial effective stress at the same depth. The initial effective stress was calculated as follows. It was obtained as the sum of the product of the unit weight and the depth of the saturated foundation ground, and the product of the unit weight and the height of the embankment. In addition, the depth from the ground surface of the foundation ground to each pore water pressure transducer was determined by dividing the average of the first 100 pore water pressure records obtained immediately before shaking by the gravitational acceleration. Finally, the embankment height was taken as the height of the embankment directly over each measurement point. Although the overall responses of Case A and Case B do not differ significantly, they are not completely identical.

At P7, the recorded values are somewhat unstable, which may be attributed to water being drawn toward the embankment, resulting in a locally drained condition. A similar situation is considered to have occurred at P4, where drainage toward the embankment may have hindered the generation and maintenance of excess pore water pressure.

In contrast, at P1 the excess pore water pressure ratio reached unity, indicating the most pronounced liquefaction. At P8 and P9, a temporary increase in excess pore water pressure was observed in Case A. Conversely, an opposite trend was identified at P3 and P4. Although sensor malfunction cannot be ruled out, these differences are considered to be influenced by local drainage conditions and the confinement of the surrounding soil, which contributed to the differing responses between Case A and Case B.

Focusing on the initial shear stress induced by the embankment, it can be confirmed that liquefaction tends to occur more easily at P1 to P3, where no initial shear stress is present, resulting in relatively large excess pore water pressure ratios. In contrast, at P8 and P9, where the initial shear stress is high, a rapid decrease in the excess pore water pressure ratio is observed. This is because the presence of initial shear stress makes the stress path during cyclic loading more likely to reach a stress state at which dilatancy occurs, and the associated volumetric expansion promotes the dissipation of excess pore water pressure. Regarding the fact that the excess pore pressure ratio at location P9 is larger than that at P6, it is considered that, at P9, the excess pore water pressure reached its peak as a result of contractive behavior before the influence of the initial shear stress became apparent. However, the results of Case A and Case B are not fully consistent, and it is therefore difficult to clearly identify common spatial trends. Additional experiments will be conducted to further evaluate the reproducibility of the observed spatial characteristics.

3.4 Vertical displacement

Figure 8 shows the time histories of the vertical displacement at the crest of the embankment. The final settlement of the embankment is the same for both cases. During shaking, the embankment crest was observed to settle while showing variations of extremely large amplitude. Such behavior is not considered realistic in actual field conditions. Therefore, it is attributed to vibration of the laser displacement sensor caused by how the fixture was attached. Nevertheless, since the vibrations eventually ceased, they did not affect the final displacement of the embankment.

3.5 Cone penetration tests

Figure 9 shows the CPT results for Case A and Case B under pre-shaking and post-shaking conditions. In both cases, the cone tip resistance under post-shaking conditions increases with depth and exceeds the pre-

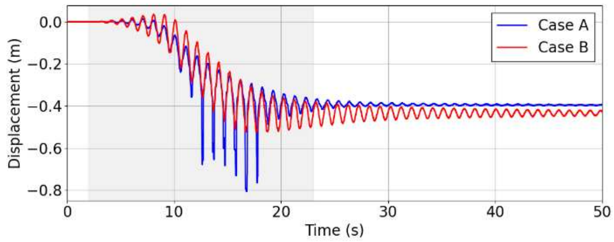

Figure 8. Vertical displacement at the crest of the embankment.

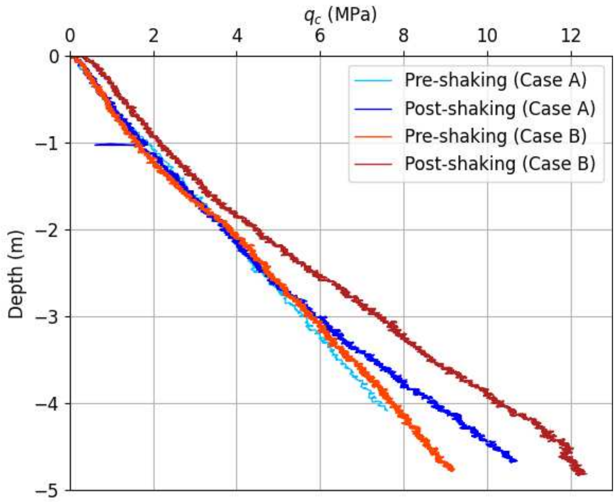

Figure 9. CPT results.

shaking values. This suggests that the soil became denser as a result of liquefaction.

Although the pre-shaking cone tip resistances for Case A and Case B are nearly identical, the post-shaking results indicate that Case A exhibits higher resistance than Case B.

4 CONCLUSIONS

In this study, the effect of wall friction was investigated by comparing cases with and without sheets attached to the container walls. As a result, significant differences were observed in the acceleration responses and CPT results, whereas no clear differences were found in the excess pore water pressure ratio or the vertical displacement at the crest of the embankment. Based on these results alone, it is difficult to determine which condition is more susceptible to liquefaction or which condition shows better agreement with numerical analysis results.

In future work, acceleration data will be compared from the viewpoint of frequency characteristics, and further comparisons with numerical analysis results will be conducted. In addition, the experiment will be repeated to confirm that no measurement issues, such as sensor malfunction, affected the results. During the repeated experiment, the orientation of the fixture will be adjusted to prevent vertical vibration of the laser displacement sensor. Furthermore, improvements will be considered to enable PIV analysis, such as using colored sand, adding reference lines on the sheets to visually capture sand deformation, or creating frame lines using colored sand.

ACKNOWLEDGEMENTS

The authors are grateful to Vargas Ruben and Katsuya Ikeno of Penta-Ocean Construction, and Tsuneo Makino and Kazuki Oshima of Penta-Techno Service, for preparing the 3D-printed formwork and Mobilon sheets. They also provided valuable expert knowledge on centrifuge model testing, which is gratefully acknowledged.

REFERENCES

Iai, S., Tobita, T. and Nakahara, T. (2005). Generalized scaling relations for dynamic centrifuge tests. *Geotechnique*, 55(5), 355-362. https://doi.org/10.1680/geot.2005.55.5.355

Okamura, M. and Inoue, T. (2012). Preperation of fully saturated models for liquefaction study. *International Journal of Physical Modelling in Geotechnics*, 12(1), 39-46. https://doi.org/10.1680/ijpmg.2012.12.1.39

Takahashi, H., Morikawa, Y., Mizutani, T., Ikeno, K., Tanaka, T., Mizutani, S., Miyoshi, T. and Hayashi, K. (2018). Technological Development of Sheet-pile Quaywall Reinforced by Geogrids. *Report of the Port and Airport Research Institute*, 57(1), 36-81.